A QM/MM Study of the Asymmetric Dihydroxylation of Terminal Aliphatic *n*-Alkenes with OsO_4·$(DHQD)_2PYDZ$: Enantioselectivity as a Function of Chain Length**

Galí Drudis-Solé,[a] Gregori Ujaque,[a] Feliu Maseras,*[a, b] and Agustí Lledós[a]

Abstract: The dihydroxylation of terminal aliphatic *n*-alkenes catalyzed by OsO_4·$(DHQD)_2PYDZ$ ($(DHQD)_2$-PYDZ = bis(dihydroquinidine)pyridazine) has been computationally studied by the hybrid QM/MM IMOMM-(Becke3LYP:MM3) method. The cases of propene, 1-butene, 1-pentene, 1-hexene, 1-heptene, 1-octene, 1-nonene, and 1-decene have been considered. A systematic treatment for the large number of possible conformations of the longer chain alkenes has been defined and applied, leading to the selection of approximately 1700 conformations to be computed. The IMOMM calculations of the transition states formed between these conformations and the catalyst generate enantiomeric excesses that closely resemble the experimental data of related systems, specifically in the preference for the *R* isomer and in its dependence on the chain length of the substrate. The selectivity increases sharply with the elongation of the short-chain alkenes until a ceiling value is reached, with further elongations having little effect on the enantiomeric excess (*ee*). These results are rationalized through the partitioning of the total energy of selected conformers, a process that leads to the identification of the most relevant regions of the catalyst and the characterization of the interactions critical for selectivity.

Keywords: asymmetric catalysis · computer chemistry · conformational search · dihydroxylation · QM/MM calculations

Introduction

The dihydroxylation of olefins with osmium tetraoxide is a powerful method with which to enantioselectively introduce chiral centers into organic substrates.[1] Its importance is remarkable owing to its common use in organic and natural product synthesis,[2,3] being also a prominent method with which to introduce two vicinal functional groups into hydrocarbons with no functional groups.[4,5] In addition, with the use of appropriate ligands in the catalyst, the enantioselectivity of the reaction can be modulated. Several research groups have recently made improvements to the catalytic dihydroxylation method.[6]

The reaction mechanism for the dihydroxylation of olefins has been a matter of controversy for a long time.[7–9] Two different mechanisms, concerted [3+2] and stepwise [2+2], have been proposed as possible mechanisms for the reaction. After the thorough work of several experimental[7,8] and theoretical research groups,[10] a scientific consensus emerged in which the [3+2] mechanism was considered to operate in the dihydroxylation of olefins by osmium tetraoxide.[11] A competitive diradical mechanism has also been discussed for the dihydroxylation of protoanemonin by osmium tetraoxide.[12] Furthermore, in very special cases and by using other metal oxides, the activation barrier for the [2+2] mechanism is lower in energy than that for the [3+2] mechanism.[13,14]

Despite its indisputable relevance, the preference for the [3+2] mechanism does not in itself provide an explanation for the stereoselectivity observed in the dihydroxylation reaction. The origin of the enantioselectivity in the dihydroxylation of olefins was previously studied by our group[15,16] by using QM/MM methods, and by other research groups.[17–19] We performed a quantitative theoretical characterization of the origin of the enantioselectivity in the dihydroxylation of aromatic olefins[15] and identified the main interactions responsible for the enantioselectivity. These inter-

[a] Dipl. Chem. G. Drudis-Solé, Dr. G. Ujaque, Dr. F. Maseras, Prof. A. Lledós
Unitat de Química Física, Departament de Química
Edifici Cn, Universitat Autònoma de Barcelona
08193 Bellaterra, Catalonia (Spain)

[b] Dr. F. Maseras
Institute of Chemical Research of Catalonia (ICIQ)
43007 Tarragona, Catalonia (Spain)
Fax: (+34) 977-92-0231
E-mail: fmaseras@iciq.es

[**] $(DHQD)_2PYDZ$ = bis(dihydroquinidine)pyridazine.

 DOI: 10.1002/chem.200400201

actions were found to be mainly π-stacking interactions between the aromatic ring of the olefin and some aromatic regions of the catalyst. Moreover, the most important regions of the catalyst involved in determining the stereochemistry were also identified.

In this work, the study was broadened to include an investigation of the origin of the enantioselectivity in the dihydroxylation of terminal aliphatic *n*-alkenes (Scheme 1).

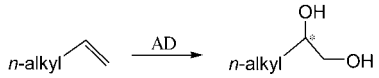

Scheme 1. Asymmetric dihydroxylation of terminal aliphatic *n*-alkenes.

The dihydroxylation of propene, 1-butene, 1-hexene, and 1-decene catalyzed by OsO_4·$(DHQD)_2PHAL$ ($(DHQD)_2PHAL$ = bis(dihydroquinidine)phthalazine) has been studied experimentally and found to be enantioselective in all cases, leading predominantly to the *R* product.[5,20] Furthermore, the experimental enantioselectivity was found to depend on the chain length of the alkene; the enantioselectivity increases sharply on going from propene to 1-pentene, and after that, the enantioselectivity remains approximately constant for 1-hexene and 1-decene. In comparison with the dihydroxylation of the aromatic olefins studied previously, the reaction of aliphatic olefins presents two main points of interest. First, the π-stacking interactions that were found to be critical for styrene cannot be responsible for the observed enantioselectivity in this case because these olefins have no aromatic rings. Secondly, the dependence of enantioselectivity on the alkene chain length has no obvious explanation. In this work, the reaction of the whole series of aliphatic terminal *n*-alkenes, from propene to 1-decene, with OsO_4·$(DHQD)_2PYDZ$ (PYDZ = pyridazine) was studied with the aim of understanding these two aspects. The computational study was carried out using the same catalyst as was used in the case of styrene to make the comparison between the two types of substrates easier. The two catalysts are in fact very similar, the only difference being in the spacer, giving practically the same enantioselectivities for the same olefins, as shown in comparative experimental studies.[21]

The calculations were carried out with the hybrid QM/MM method, IMOMM,[22] which is closely related to the ONIOM method.[23] This method was used in previous computational studies of dihydroxylation reactions,[15,16] and has also been used successfully in other computational studies of homogeneous catalysis.[24–26]

The computational study of these aliphatic systems is much more complicated than that of aromatic olefins owing to the large number of conformations that aliphatic *n*-alkenes can achieve. Because of this, the first three sections of the results will deal with the problems of identification and screening of the possible conformations. Afterwards, sections are dedicated to a comparison of the computed enantioselectivities with experimental values, the partitioning of the total energy differences, the identification of the critical regions of the catalyst for the reaction and a qualitative analysis of the chemical nature of the key interactions. The last section will summarize the conclusions.

Abstract in Catalan: *La dihidroxilació asimètrica d'olefines terminals catalitzada per OsO_4·$(DHQD)_2PYDZ$, ha estat estudiada computacionalment utilitzant el mètode híbrid QM/MM IMOMM(B3LYP:MM3). Degut al gran número de conformacions presents a les olefines estudiades, propè, 1-butè, 1-pentè, 1-hexè, 1-heptè, 1-octè, 1-nonè i 1-decè, hem proposat una metodologia sistemàtica que ens ha permès seleccionar aproximadament 1700 conformacions. Els càlculs IMOMM d'aquests 1700 confòrmers ens han permès predir computacionalment els excessos enantiomèrics esperats. Aquests concorden amb els valors experimentals, a més de reproduir la seva dependència amb la longitud de la cadena. Així, s'obtenen increments pronunciats de l'enantioselectivitat si s'allarguen cadenes curtes, tot i que a partir d'una certa llargària, la seva elongació té pocs efectes sobre l'enantioselectivitat. Aquest fet s'explica a través de la partició de l'energia efectuada sobre els confòrmers seleccionats, que ha permès a més a més, identificar les regions del catalitzador que més contribueixen a l'enantioselectivitat de la reacció.*

Computational Methods

IMOMM[22] calculations were performed with a program built from modified versions of two standard programs: Gaussian98[27] for quantum mechanics calculations (QM) and MM3(92)[28] for the molecular mechanics calculations (MM). Becke3LYP[29] was always used for the QM description and was applied to the OsO_4·NH_3+CH_2=$CHCH_3$ fragment; the rest of the system was described by means of the MM3(92) force field.[30] Preliminary tests with a smaller QM region, OsO_4·NH_3+CH_2=CH_2, were shown to give poorer agreement with experiment. van der Waals parameters for the osmium atom were taken from the UFF force field,[31] and torsional contributions, including dihedral angles with the metal atom in the terminal position, were set to zero. The MM dipole moments for the carbon–oxygen bonds being formed were set to zero in most calculations. An additional set of calculations (vide infra) were carried out by using the MM3 value for a carbon–oxygen(alcohol) bond to check that this approximation was reasonable. All geometrical parameters were fully optimized without symmetry restrictions except for the bond distances between the QM and MM regions of the molecules. The parameters were frozen at 1.015 (N–H) and 1.101 (C–H) Å in the QM part, and at 1.448 (N–C) and 1.434 (C–C) Å in the MM part.

The basis set I used for the molecular orbital calculations was 6-31G(d) for the oxygen atom,[32,33] and 6-31G for the nitrogen, carbon, and hydrogen atoms;[33] the inner electrons of the osmium atom were described by the LANL2DZ effective core potential (ECP),[34] whereas the outer electrons were described using the double-ξ approach associated with the corresponding ECP, also called LANL2DZ. This basis set has been proven to properly describe this system.[35] In addition, single-point calculations at the CCSD(T) level in the QM region of the lowest energy conformations of the *R* and *S* transition states of propene, 1-hexene, and 1-decene were also performed by using the basis set II. The basis set II was the same as that described above for the osmium atom, with the addition of a set of f functions (exponent 0.886),[36] and the 6-311g+(d) basis set

was used for the rest. The energy differences between both methods and basis set are minimal (see text).

Results and Discussion

Approach of the olefin to the catalyst: In the [3+2] mechanism the olefin can approach the catalyst in several different ways, and in order to investigate all the possible transition states associated with the formation of the five-membered osmate ester ring, one must take all of them into account. These different paths are classified according to the criteria depicted in Figure 1. Figure 1a shows the top view along the

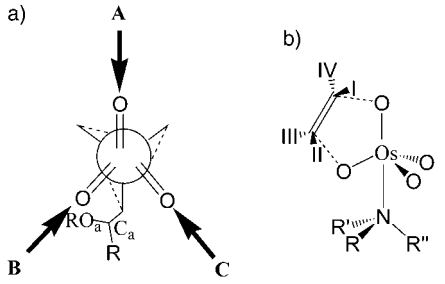

Figure 1. The possible reaction pathways in the IMOMM calculations. a) Top view along the O–Os–N axis showing the three different regions (**A**, **B**, and **C**) of approach of the olefin. b) Side view perpendicular to the O–Os–N axis showing the four possible orientations (**I**, **II**, **III**, and **IV**) of the alkene substituent.

O–Os–N axis of the possible regions of approach of the olefin to the catalyst. The catalyst has a trigonal bipyramidal coordination around the metal center with three oxygen ligands in equatorial positions and one amine ligand and one oxygen ligand in apical positions. The equatorial oxygen atoms O(Os) are staggered with respect to the amine substituents C(N). The alkene forms bonds with one of the equatorial oxygen atoms and the axial oxygen atom. Since the three equatorial oxygen atoms are not equivalent, the approach of the olefin to each of them defines a distinct family of reaction paths, which are labeled **A**, **B**, and **C** according to the notation proposed by Sharpless and co-workers,[8b,c] and as used in our previous studies.[15]

A second question is the placement of the olefin substituent, an aliphatic chain in this study, which can be located in four different orientations. These four orientations, labeled as **I**, **II**, **III**, and **IV**, are shown in Figure 1b. The three regions of approach and the four possible positions of the olefin substituent per region yield a total of 12 different ways in which the reaction can proceed. The overall selectivity of the reaction depends on the orientation of the substrate. When the orientation is **I** or **III**, the final diol product is the *R* enantiomer, whereas for orientations **II** and **IV** the final product is the *S* enantiomer.

Once the different pathways for the approach of the olefin to the catalyst have been identified, one faces a much more complicated problem in dealing with the conformations of the olefins under study. All of these reaction pathways are going to be studied for each member of a series of *n*-aliphatic alkenes, from propene to 1-decene. The propene molecule has only one conformation, but as the chain length becomes longer, the number of conformations increases dramatically, and can be in the order of thousands for the case of 1-decene. In addition, each of the olefin conformations needs to be studied for each of the 12 different pathways, and the relative stability of these conformations is also affected by their interactions with the catalyst. The calculation of such a large number of transition states is unfeasible even if QM/MM methods are applied because this system requires an ab initio level for the QM part. Hence, we need to develop a strategy that will screen all the possible conformations and concentrate the computational effort only on the most stable conformations since only these conformations will be involved in the reactive pathways. The next section is dedicated to a description of the strategy adopted to deal with this issue.

Conformational search of the "catalyst+olefin" systems: For any molecule, the presence of geometrical arrangements of similar energy separated by low energy barriers, known as conformers, seriously complicates the analysis of the chemical properties of any system. For example, long-chain aliphatic 1-alkenes, such as decene, have a large number of conformers of similar energy with low energy barriers owing to rotation around the C–C single bonds. Therefore, a proper conformational analysis is crucial to the computational treatment of the enantioselectivity of these systems. The importance of conformational analysis for catalyzed dihydroxylation processes in other systems has already been pointed out by other authors.[18,19]

For the dihydroxylation of aliphatic *n*-alkenes with OsO_4·$(DHQD)_2PYDZ$ one can regard the system as being composed of two different parts, the catalyst and the olefin. As far as the catalyst is concerned, two different conformations have been taken into account. Even though the catalyst is a large molecule, it has several quite rigid aromatic fragments that significantly reduce the number of possible conformations. Moreover, a previous theoretical analysis of this catalyst has shown that one of the studied conformations is preferred.[15] In addition, experimental studies (NMR, NOESY, etc.) carried out by Corey and Noe[37] on this catalyst and by Sharpless and co-workers[38] on a very similar catalyst, OsO_4·$(DHQD)_2PHAL$, have also shown that this is quite a rigid molecule. The second conformation considered implies the rotation of one of the quinoline rings, which might enhance the interactions between the ligand and the longer olefins, and has also been considered by other authors.[15,37,38] Both structures present a U-shape conformation which was shown to act as a binding site when the olefin is styrene.[15]

As far as the alkenes under study are concerned, the large number of conformations that the olefin substituent (an aliphatic chain) can adopt, especially when the chain length is

long, makes the problem more complicated. In addition, in this case, the stability of an olefin conformation is also affected by the interactions between the olefin substituent and the catalyst, which thus has to be included in the conformational search. Several methods for performing the conformational analysis have been proposed, and the one we used follows a scheme based on the "systematic search" approach.[39] Our treatment consisted of two parts. First we developed a method to identify all the possible conformations. Afterwards, we screened all these possible conformations so that we only performed the relatively expensive QM/MM calculations on the most stable ones.

We were thus interested in identifying the possible conformations of the transition states formed between each 1-alkene from propene to 1-decene and the catalyst. The generation of the different conformations of an olefin with a chain length of "n+1" carbon atoms is based on the conformations of the previous olefin which has a chain length of "n" carbon atoms. The construction of an olefin with "n+1" carbon atoms implies the addition of a methyl substituent onto the terminal methyl group of the olefin with "n" carbon atoms. The terminal group of the "n" olefin has three hydrogen groups, and the possibility of the methyl group replacing each of them is considered. Consequently, for each available conformer of the "n" olefin, three conformers of the "n+1" olefin have to be considered. For instance, to build up the different conformers of 1-butene, each of the three hydrogen atoms of the terminal methyl group of propene have to be subsequently replaced by a new CH_3 group (Figure 2). This is the general scheme used for the construction of the different conformations of the terminal aliphatic n-alkenes on going from propene to 1-decene.

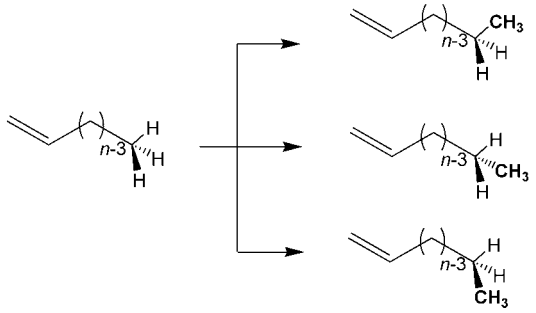

Figure 2. Schematic representation of the method used for conformer generation.

This algorithm is suitable for the systematic identification of a large number of conformations, and is very likely to include the most stable ones, but has the serious problem of involving a very high number of structures. The number of conformations increases exponentially with the length of the chain. For propene there are the 12 possible structures (corresponding to the region of approach and the orientation of the olefin with respect to the catalyst) as discussed in the previous section. For 1-butene, the number increases to 36, that is, 3 times 12. As the chain lengthens, the number of conformations grows very quickly, 108 for 1-pentene, 324 for 1-hexene, 972 for 1-heptene, 2916 for 1-octene, 8748 for 1-nonene, and 26244 for 1-decene. Therefore, there are almost 40000 different conformers. One mode of approach of the olefin to a second conformation of the catalyst was also studied, thus increasing the total number of conformers to 53000. The IMOMM(Becke3LYP:MM3) calculation of all of these transition states is not feasible. Instead, we decided to select the transition states that would be fully optimized by the IMOMM method.

The screening was based on the MM energies obtained by IMOMM(Becke3LYP:MM3) optimizations with the QM region frozen. Because of the definition of the IMOMM method, such a calculation can be done purely at the much cheaper MM level, with the QM energy being added afterwards. The saving in computational effort is substantial; the MM optimization of a given geometry takes only about 15 seconds of computer time, and the corresponding IMOMM(B3LYP:MM3) calculation requires about 5 h of computer time. The starting conformations of a given olefin, for instance 1-butene, were obtained from the optimized conformations of the preceding one, in this case, propene, following the procedure explained above. Then, once the conformations had been generated, they were submitted to a restricted MM optimization: the atoms belonging to the QM region were kept frozen, whereas the atoms of the MM region were fully optimized at the molecular mechanics level. The geometrical dispositions of the atoms in the QM region were taken from the IMOMM-optimized transition state of the "catalyst+propene" system since propene is described in the QM part. The geometrical parameters of this transition state in the QM region were kept frozen throughout the conformational search. A schematic representation of the procedure used to perform the conformational calculations for the complete series of olefins is presented in Figure 3.

Following the systematic search described above, the conformational space for the different "olefin+catalyst" systems on going from propene to 1-decene was evaluated at the MM level. The next step was to decide which conformers had to be considered in the IMOMM calculations. To choose a reasonable criterion, the enantiomeric excess for each of the olefins was estimated by using the energy values obtained from the conformational search at the MM level. The *ee* was calculated for several scenarios, by considering up to 99, 198, 300, and 399 conformers for each of the olefins from propene to 1-decene. These conformers were chosen as the most stable from each region of approach (**A**, **B**, and **C**, Figure 1). One third was taken from each region to ensure that the effect of eventual large rearrangements in the QM region was included. The results obtained by taking up to 300 or up to 399 conformers were practically the same. Hence, we decided to select 300 conformations for the IMOMM calculations. Thus, the total number of conformers considered in the IMOMM calculations was all the possible

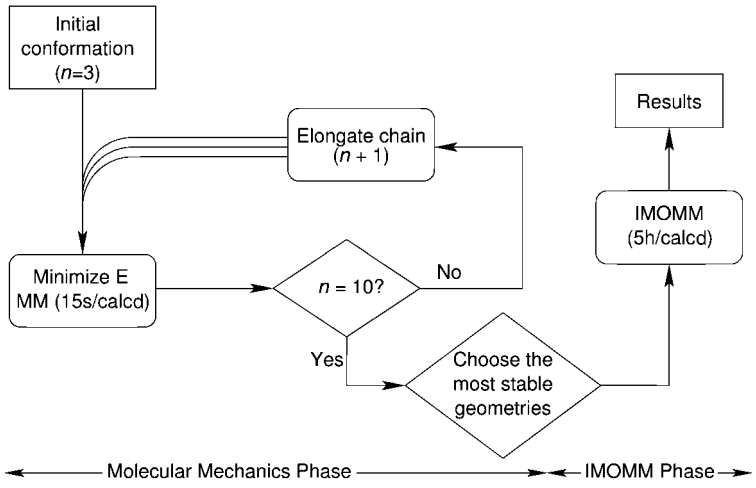

Figure 3. Flux diagram for the systematic conformational search of the complete series of olefins.

ones for propene to 1-pentene (16 for propene, 48 for 1-butene, and 144 for 1-pentene) and 300 for each olefin from 1-hexene to 1-decene.

In energy terms, the selection criteria mean that in the case of 1-heptene those conformers with a relative energy higher than 4.4, 3.2, and 3.5 kcal mol^{-1} for each of the three regions, respectively, were rejected. Remember that 100 conformations were selected for each of the regions. In the case of 1-octene, the cut-off energies were 3.1, 2.7, and 2.4 kcal mol^{-1}, respectively. For 1-nonene these energies were 2.9, 3.0, and 2.7 kcal mol^{-1}, respectively, and for 1-decene the cut-off energies were 2.7, 3.0, and 2.9 kcal mol^{-1} for each of the regions, respectively. To put these relative energies into perspective, let us mention 1-octene as an example; the conformer with an energy 2.4 kcal mol^{-1} above the most stable conformer contributes only 0.13% to the total population of the region **C** of 1-octene in our specific study. As a result, the final number of transition states optimized at the IMOMM level was approximately 1700. The results presented in next sections are based on these calculations at the IMOMM level.

Computational evaluation of enantioselectivity: Computational studies were carried out on the complete series of olefins, from propene to 1-decene. The catalyst used was OsO_4·$(DHQD)_2PYDZ$. For each catalyst–substrate pair all possible conformations of the olefin were screened by following the procedure described in the previous section, and the more stable conformations (up to 300 for the longer substrates) were fully optimized as transition states by the IMOMM method. The energies resulting from these geometry optimizations were then used to estimate computationally the enantiomeric excesses by assuming that the ratio of the products follow the Maxwell–Boltzmann distribution of the energies of the corresponding transition states, as is often the case in this type of calculation.[15,26,40] The analysis was carried out by using different numbers of conformations to further check that enough of them had been included.

Our approach to the calculation of the enantiomeric excess can be viewed as the performance of an ensemble average over a canonical ensemble in which the conformations are systematically enumerated. The same result can also be obtained by molecular dynamics simulations in which a time average is carried out. In practice molecular dynamics are used more often for this type of computational evaluation because it is impossible to enumerate the conformations when the system becomes too large. However, we feel that when the enumeration of conformations is possible, as here, the present approach is more transparent, and it avoids the intrinsic problems of equilibration and the choice of dynamic parameters used in the molecular dynamics simulations.

The results presented in Table 1 confirm that the total number of conformations considered in the calculations of the enantiomeric excess for each of the olefins is sufficient to obtain reliable computational values. With propene, 1-butene, and 1-pentene, all the possible conformations were considered. For 1-hexene to 1-decene, however, only up to 300 conformations were selected, as indicated in the previous section. The results in Table 1 show that for longer-chain olefins when the number of conformations considered increases from 1 to 200 the calculated *ee* decreases, but when the number of conformations considered is more than 200 the calculated *ee* is shown to have already converged, and remains practically constant.

At this point, it is worth mentioning that although certainly not all the computed conformations contribute significant-

Table 1. The enantiomeric excess as a function of the number of conformers used in the IMOMM-(B3LYP:MM3) analysis. Results for olefins between propene (C3) and 1-decene (C10) are presented.

Number of conformations	Enantiomeric excess							
	C3	C4	C5	C6	C7	C8	C9	C10
1	100	100	100	100	100	100	100	100
5	46	69	83	100	100	100	100	100
20	43	57	70	88	95	100	100	100
50		55	67	84	90	95	96	99
100			66	83	86	89	91	93
200				82	86	88	89	90
250				82	86	88	89	90
total	43	55	66	82	86	88	89	90

ly to the overall selectivity, quite a few of them do. In fact, with propene the most stable transition state accounts for only 50% of the product, 41% with 1-butene, 33% with 1-pentene, 33% with 1-hexene, 24% with 1-heptene, 25% with 1-octene, 17% with 1-nonene, and 10% with 1-decene. These results demonstrate that a systematic conformational analysis is needed in order to obtain accurate *ee* values. For instance, in the case of 1-decene, the most stable conformation accounts for only 10% of the product, giving 100% *ee*. The 20 most stable conformations account for 66% of the total product, also giving 100% *ee*. In both cases, that is, with 1 or 20 conformations, the calculated *ee* is 100%, which means that there are no *S* conformations amongst the 20 most stable structures. The 50 most stable conformations account for 86% of the total product. In this case, some *S* enantiomers are also formed, and the calculated *ee* decreases to 99%. The 200 most stable conformers account for 99% of the products, and the calculated value for the *ee* is 90%. At this point, most of the conformations that contribute to the *ee* have been considered, and the inclusion of more conformations does not modify the enantioselectivity. Therefore, in order to calculate an accurate value for the *ee*, a large number of conformations (at least 200) are needed to account for 99% of the product. Similar results were found for the other long-chain olefins. This is in complete contrast with what happened in the previously studied case of styrene,[15] for which there was no conformational problem. These results underline the necessity of a systematic conformational analysis in the current case.

To confirm the quality of the QM description, single-point calculations at the CCSD(T) level of theory using a larger basis set were performed on the most stable transition states that give the *R* and *S* products for propene, 1-hexene, and 1-decene. The energy differences between the most stable *R* and *S* transition states at the B3LYP level are 0.2, 1.1, and 0.5 kcal mol^{-1} for propene, 1-hexene, and 1-decene, respectively. In the case of the CCSD(T) calculations, these energy differences for the same alkenes are 0.2, 0.9, and 0.5 kcal mol^{-1}, respectively. The energy differences determined by the two methods are very similar, further validating the method and basis set used.

Comparison between computed and experimental observations: The experimental study of the dihydroxylation of a series of aliphatic *n*-alkenes shows that the observed enantioselectivity depends on the olefinic chain length (Figure 4).[3,20] The catalyst used in the experiments was OsO_4•$(DHQD)_2PHAL$ and the olefins studied were propene, 1-butene, 1-pentene, 1-hexene, and 1-decene. The *R* enantiomer was always found to be the major product in the dihydroxylation of this series of aliphatic *n*-alkenes. When varying the olefin from propene to 1-decene the observed enantiomeric excess increases from approximately 35 to nearly 85%. The enantioselectivity initially increases significantly with the number of carbon atoms (from propene to pentene), reaching a ceiling saturation value when the chain length is greater than five. Consequently, the selectivity for 1-pentene, 1-hexene, and 1-decene is practically the same.

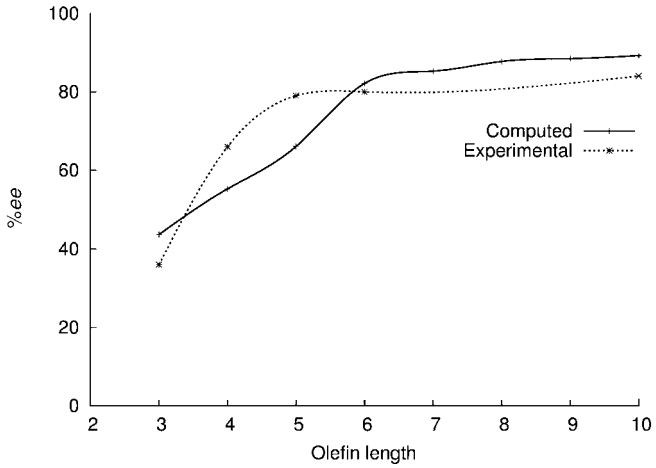

Figure 4. Experimental[2,20] and computed enantiomeric excesses as a function of the chain length of the aliphatic *n*-alkenes.

The computed enantiomeric excesses, together with the experimental values, for each of the substrates considered, are presented in Figure 4. The computed results for the *ee* are in excellent agreement with the experimental values. The calculations are able to reproduce the experimentally observed increase in the *ee* of the short-chain olefins and the presence of a ceiling value after which the increase in enantioselectivity is much smaller. Moreover, even the *ee* values derived from the IMOMM calculations are quite similar to the experimental values, the largest difference corresponding to 1-pentene (computed 66% versus experimental 79%). The saturation value is reached with 1-pentene in the experimental study, but with 1-hexene in the calculations, however, we consider this to be a minor discrepancy.

As far as the region of entry of the olefin is concerned, the most stable transition states for each of the olefins from propene to 1-decene that give the *R* enantiomer have the olefin located in region **B**. In particular, the most stable conformations correspond to the **B-III** orientation. Similar results were obtained for the *S* enantiomer, for which the most stable conformation is, in most cases, **B-IV**. The preference for entry at region **B** has already been observed experimentally.[8b] This preference over other regions reflects the nature of the steric interactions between the catalyst and substrate. Regions **A** and **C** are less crowded than region **B**. Therefore, the magnitude of the steric interactions should be smaller in these regions than in region **B**. Nevertheless, the saddle-point energy is lower in region **B** than in the others, which indicates that the steric interactions are of an attractive nature. This fact was also observed for the aromatic alkenes,[15] and does not contradict the existence of an intermediate in the reaction path previously identified.[16a]

The energy terms that differentiate *R* and *S* enantiomers: Having shown that the experimental trends are properly re-

produced by calculation, we then sought to explain them. To discern the main differences between the *R* and *S* enantiomers it is first necessary to separate the total energy into its components and to identify which of them is responsible for the difference between the paths leading to the *R* and *S* products. We start by distinguishing the energies of the QM and MM parts of these calculations.

The energy of the QM part is quite similar and within the same range for the different conformations of the *R* and *S* transition states for each of the olefins. For instance, in the case of 1-decene the QM energies for the *R* structures are between −1.2 and 1.3 kcal mol^{-1} with respect to that of the most stable QM/MM isomer, and for the *S* structures they are between −1.1 and 0.5 kcal mol^{-1}. No significant differences can thus be observed, either in the range or in the average of the relative QM energies of the *R* and *S* structures. Things are different for the MM energies. In this case, the corresponding values are 0.0 and 6.2 kcal mol^{-1} for the *R* conformers and 2.1 and 6.0 kcal mol^{-1} for the *S* conformers. The difference between the lowest relative MM energies is 2.1 kcal mol^{-1}. That is, the most stable *S* isomer will have an MM energy at least 2.1 kcal mol^{-1} above that of the most stable *R* isomer. An energy difference of 2 kcal mol^{-1} is certainly significant for the enantioselectivity, and because of this, we will focus our analysis on the MM energies. Moreover, the range of energies is significantly wider for the MM than for the QM values, which further indicates that most of the energy difference between the conformers lies in the MM part.

The next logical step is to separate the MM energy into its components. The procedure here is however complicated by the large number and variety of relevant conformations. The diversity of the structures makes the application of the dispersion criterion used above to discard the QM contribution impossible. The ideal study would consist of an exhaustive analysis of all the conformations that contribute to the enantioselectivity of each of the olefins. However, owing to the large number of conformations to be considered, this is impractical. Instead, we decided to analyze in detail some of the most stable conformations of the *R* and *S* enantiomers of the olefins of the series. Although the optimal analysis would involve a consideration of all the conformations, we still expect this analysis to be informative. Hence, we will focus on two selected single conformations (which are among the most stable conformations) of the *R* and *S* enantiomers of each of the olefins from propene to 1-decene.

The different contributions to the MM energy of each of the selected conformers are given in Table 2. The energy differences between the *R* and *S* enantiomers for the compression, bending, torsional, dipole–dipole, and cross terms are small relative to the energy differences for the van der Waals term. The differences in the compression, bending, dipole–dipole, and cross terms are 0.2 kcal mol^{-1} at most. The differences in the torsional term can be somewhat larger, up to −0.8 kcal mol^{-1}, but they are never more than 35 % of the total energy difference. It is clear from Table 2 that the van der Waals term is the main cause of the energy differences between the *R* and *S* enantiomers. The real meaning of this term in the MM3 force field, as in most force fields, cannot be directly assigned to the physical meaning of the van der Waals interactions[41] because of the parameter fitting involved in the force-field development. In any case, without defining exactly the meaning of the term here, in these calculations it clearly includes the origin of enantioselectivity, and we will use it to analyze the main differences between the different conformations.

It may seem surprising that electrostatic interactions do not have more influence on the enantioselectivity. This is essentially because of the nature of the MM3 force field. The charge on all the atoms in the MM region of the molecule is zero by definition of the atomic types. Hence all the eventual charge–charge terms in the IMOMM QM/MM calculation cancel out. Charges in the QM region (notably on the osmium center) are arbitrarily set to zero on the assumption that they would not be able to discriminate between enan-

Table 2. Breakdown of the MM energy into its component terms for selected conformations of the transition states associated with each of the olefins in the series.

Olefin		MM energy [kcal mol^{-1}]					
		compression	bending	VdW	torsional	dipole–dipole	cross-terms
C3	*R*	6.7	19.9	61.9	24.2	3.0	−0.8
	S	6.7	19.9	62.7	24.2	3.0	−0.8
	Diff (*R*−*S*)	0.0	0.0	−0.8	0.0	0.0	0.0
C4	*R*	6.7	20.1	62.7	23.7	2.8	−0.9
	S	6.7	20.0	63.6	24.0	2.8	−0.8
	Diff (*R*−*S*)	0.0	0.1	0.9	−0.3	0.0	−0.1
C5	*R*	6.8	20.2	62.7	23.8	2.7	−0.9
	S	6.7	20.1	64.4	24.0	2.8	−0.8
	Diff (*R*−*S*)	0.1	0.1	−1.7	−0.2	−0.1	−0.1
C6	*R*	6.8	20.2	62.6	23.7	2.8	−0.8
	S	6.8	20.1	65.1	24.0	2.8	−0.8
	Diff (*R*−*S*)	0.0	0.1	−2.5	-0.3	0.0	0.0
C7	*R*	6.9	20.3	63.2	23.7	2.8	−0.8
	S	6.8	20.1	65.2	24.5	3.0	−0.8
	Diff (*R*−*S*)	0.1	0.2	−2.0	-0.8	−0.2	0.0
C8	*R*	6.9	20.3	63.7	23.7	2.8	−0.8
	S	6.9	20.1	66.0	24.6	3.0	−0.8
	Diff (*R*−*S*)	0.0	0.2	−2.3	−0.8	−0.2	0.0
C9	*R*	7.0	20.4	64.5	23.8	2.8	−0.8
	S	6.9	20.2	66.9	24.6	3.0	−0.8
	Diff (*R*−*S*)	0.1	0.2	−2.4	−0.8	−0.2	0.0
C10	*R*	7.0	20.4	65.3	23.8	2.8	−0.8
	S	7.0	20.2	67.8	24.6	3.0	−0.8
	Diff (*R*−*S*)	0.1	0.2	−2.4	−0.8	−0.2	0.0

tiomers, thus eliminating the possibility of charge–dipole terms in the QM/MM calculation. As a result, the MM3 electrostatic contribution is reduced to the dipole–dipole interactions. This dipole–dipole term is given in Table 2, in which it can be seen that this term is not negligible from an absolute point of view, with values close to 3 kcal mol^{-1}, but that it is essentially the same for all of the *R* and *S* enantiomers. The fact that the interactions labeled as electrostatic by the force field are not more critical for enantioselectivity has no direct implication on the real nature of the critical interactions. In fact, if a difference force field was applied, electrostatic interactions would likely account for a substantial part of the difference.

A significant part of the dipole–dipole interaction could in principle be associated with the dipole moment of the C–O bond being formed, which is not well defined a priori by the force field. It was mentioned in the Computational Methods section that the value for this dipole moment was set to zero for most calculations, including those presented above. In order to check whether this approach was critical, an additional set of calculations were carried out with a different value for this dipole moment, in particular, the value corresponding to a standard carbon–oxygen(alcohol) bond in the MM3 force field. Pure MM calculations were carried out on frozen QM geometries for the particular case of region B. These calculations were of the same type as those reported above for the screening of the conformations. The computed *ee* values for the alkenes from 1-butene to 1-decene were 55, 66, 78, 78, 79, 83, and 85 for the zero dipole moment and 54, 66, 76, 78, 81, 85, and 88 for the non-zero dipole moment. The particular value of this dipole moment thus has a very minor influence on the computed enantiomeric excess. Given the results of this preliminary test at a pure MM level, no further studies were carried out at the more expensive QM/MM level on this issue.

The van der Waals contribution is a summation of the interactions between atom pairs. Thus, it is straightforward to separate this term into interactions between two or more sets of atoms. We have partitioned the system into two fragments, the catalyst and the substrate, and separated the total van der Waals interaction into three blocks, those between the atoms in each fragment (catalyst–catalyst and substrate–substrate) and those between the two fragments (catalyst–substrate). This scheme was applied to the selected conformations of each of the considered olefins and the results are collected in Table 3. Not surprisingly, the interaction between the two fragments, the catalyst and the substrate, is the key term, and can faithfully explain the variation in *ee* with increasing alkene chain length; the sharp increase in the selectivity from propene to 1-hexene and the subsequent slow increase from 1-hexene to 1-decene. We have thus concentrated all subsequent analyses on this particular term, the van der Waals interaction between the catalyst and the substrate.

The key regions of the catalyst: In the previous section, the overall energies of selected conformations of catalyst–substrate pairs were analyzed, and the main differences between the enantiomers was identified as being associated with the van der Waals interaction between the catalyst and substrate. This term will be analyzed in detail in this section.

Table 3. MM3 van der Waals interaction energies between the catalyst and the olefin fragments of selected conformations of the transition states.

Olefin		VdW energies [kcal mol^{-1}]			
		cat.–cat.	subs.–subs.	cat.–subs.	total
C3	*R*	66.5	0.0	−4.6	61.9
	S	66.6	0.0	−3.9	62.7
	Diff (*R*−*S*)	−0.1	0.0	−0.7	−0.8
C4	*R*	67.2	1.1	−5.7	62.7
	S	67.0	1.0	−4.4	63.6
	Diff (*R*−*S*)	0.2	0.1	−1.2	−0.9
C5	*R*	67.2	2.1	−6.6	62.7
	S	67.0	2.0	−4.6	64.4
	Diff (*R*−*S*)	0.2	0.1	−2.0	−1.7
C6	*R*	67.4	3.1	−7.9	62.6
	S	67.0	2.9	−4.9	65.1
	Diff (*R*−*S*)	0.4	0.2	−3.0	−2.5
C7	*R*	67.5	4.0	−8.3	63.2
	S	66.7	4.1	−5.6	65.2
	Diff (*R*−*S*)	0.8	−0.1	−2.7	−2.0
C8	*R*	67.5	5.0	−8.7	63.7
	S	66.7	5.1	−5.7	66.0
	Diff (*R*−*S*)	0.8	−0.1	−3.0	−2.3
C9	*R*	67.5	5.9	−8.9	64.5
	S	66.7	6.0	−5.8	66.9
	Diff (*R*−*S*)	0.8	−0.1	−3.1	−2.4
C10	*R*	67.5	6.9	−9.0	65.4
	S	66.7	7.0	−5.8	67.8
	Diff (*R*−*S*)	0.8	−0.1	−3.1	−2.4

The interaction energy between the olefins and the catalyst in the transition states for the *R* and *S* products are presented in Figure 5. The interaction energy for the *R* enantiomer increases across the series of olefins, though the increase is larger on going from propene to 1-hexene than for the rest of the olefins in the series. For the *S* enantiomer, in contrast, the interaction energy increases slowly and con-

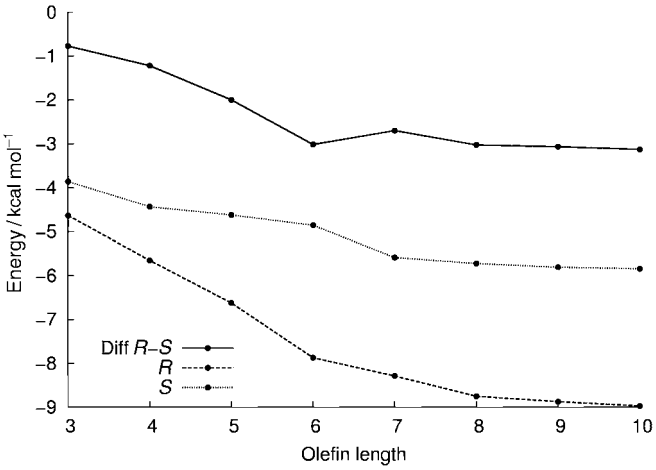

Figure 5. MM3 van der Waals interactions (kcal mol^{-1}) between the catalyst and olefins in the selected conformers.

stantly for all the olefins studied. Figure 5 also shows the difference between the interaction energies of the transition states of the *R* and *S* enantiomers and allows the variation in the enantioselectivity as a function of the chain length to be explained. The interaction energy increases more rapidly for the *R* transition states than for the *S* transition states until the chain has six carbon atoms. After this point, the interaction energy increases very smoothly and similarly for both enantiomers such that the enantioselectivity remains practically constant, hence displaying saturation behavior. Hence, for the first part of the series, the enantioselectivity of the reaction increases with increasing chain length because the attractive interactions between the olefin and the catalyst increase more rapidly for the *R* enantiomer than for the *S* enantiomer in their respective transition states.

We can go one step further in the analysis of the interaction between the substrate and catalyst, and evaluate the interaction energies between the series of olefins and different parts of the catalyst separately. The catalyst has been divided into five parts (Figure 6). These parts are labeled as Quinoline A, Quinoline B, PYDZ, Quinuclidine A, Quinuclidine B, and OsO_4.

The interaction energies between selected conformers of the whole series of olefins and each of the different parts of the catalyst are shown in Figure 7. The part of the catalyst that has the largest interaction with the olefins is Quinoline A; it accounts for more than 40% of the total interaction in the transition state for the *R* enantiomer and about 60% for the *S* enantiomer. This interaction increases more rapidly between propene and 1-hexene than between 1-heptene and 1-decene. Nevertheless, it behaves very similarly for both enantiomers. Therefore, even though Quinoline A is decisive for catalytic purposes, it is responsible for neither the enantioselectivity nor its dependence on the chain length. In the analysis performed on the aromatic olefins this was also the principal energy term, but in that case, it could also explain the enantioselectivity.[15] Therefore it appears there is a significant difference in the way in which the catalyst interacts with the two types of substrates.

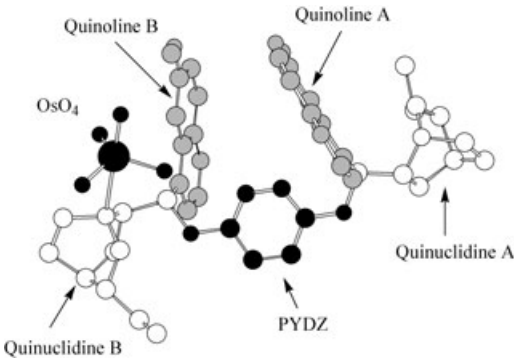

Figure 6. The different regions of the OsO_4·$(DHQD)_2$PYDZ catalyst. Hydrogen atoms are omitted for clarity.

For the *R* enantiomers, the spacer PYDZ makes the second largest contribution to the interaction energy of the transition states. For this enantiomeric form, the interaction between the olefins and PYDZ behaves similarly to that of the interaction with Quinoline A; it increases markedly on going from propene to 1-hexene, and after that, it remains approximately constant for the rest of the series up to 1-decene. In the case of the *S* enantiomers, in contrast, the PYDZ region is not so relevant, and the energetic contribution of this part of the catalyst is at most of the same order as the other less relevant parts of the catalyst (Figure 7). This indicates that the PYDZ region is one of the key factors that differentiate the interactions between the olefins and the catalyst in the transition states of the *R* and *S* enantiomers. Therefore, PYDZ is important in determining the enantioselectivity of these reactions in contrast to what was found for aromatic olefins.[15]

Quinuclidine B also requires special mention. The interaction between this part of the catalyst and the olefins in the transition states of the *R* products is significant. This interaction increases markedly on going from propene to 1-hexene, its increase being more gradual for the rest of the series of the olefins. In contrast, this interaction is almost negligible relative to those of the other parts of the catalyst in the transition states that give the *S* products. This is another

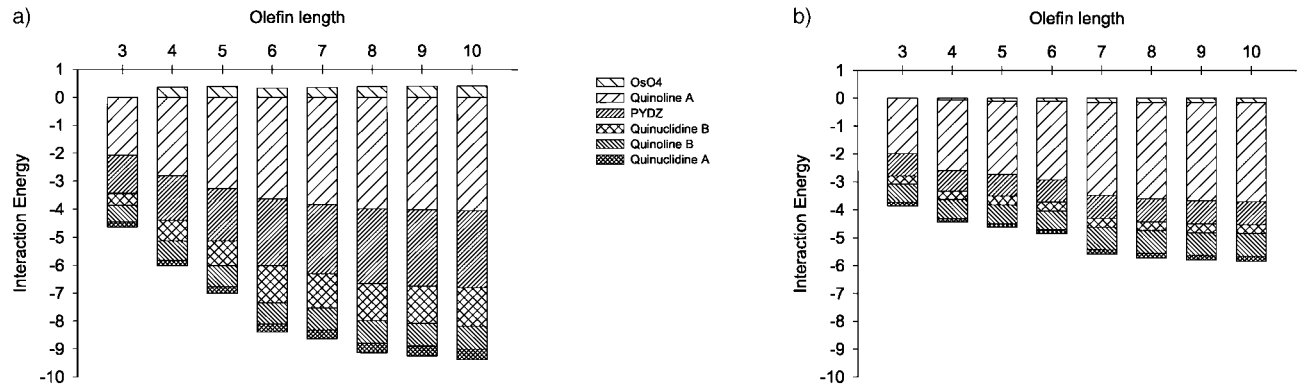

Figure 7. van der Waals interactions between the aliphatic *n*-alkenes and the different regions of the catalyst for the selected conformers: a) *R* enantiomers and b) *S* enantiomers.

factor that differentiates the interactions between the olefins and the catalyst in the transition states of the *R* and *S* enantiomers. Therefore, Quinuclidine B also helps to determine the stereochemistry of the products derived from the aliphatic *n*-olefins. Again, in the case of the dihydroxylation of aromatic olefins this interaction was not essential.[15]

The interactions between the olefins and the remaining parts of the catalyst, Quinoline B, OsO_4, and Quinuclidine A, are quite small in all cases relative to those mentioned above. All of these interactions are quite similar for all of the olefins and are independent of the chain length. Moreover, their values are also similar for both the *R* and *S* transition states. Therefore, these regions of the catalyst do not contribute significantly to the enantioselectivity or the catalysis of the reaction.

The enantioselectivity of the dihydroxylation of aliphatic *n*-alkenes is therefore determined by the interactions of the olefin with two regions of the catalyst: PYDZ and Quinuclidine B. In the transition states that lead to the *R* products, the interaction of the olefin with each of these two regions depends strongly on the olefin chain length. For all of these transition states, and especially for the interaction with the PYDZ moiety, results prove that on going from propene to 1-hexene this dependence is much more pronounced than on going from 1-heptene to 1-decene. The overall effect of these two catalytic regions is a rapid increase in the difference in stability between the *R* and *S* transition states when going from propene to 1-hexene, and a much more gradual increase on going from 1-hexene to 1-decene. This behavior closely reproduces that of the total van der Waals interactions (Table 1), and of the total energy difference (Figure 5). Therefore, the enantioselectivity and its dependence on chain length can be traced in these IMOMM(Becke3-LYP:MM3) calculations to the van der Waals interactions of the olefin with these two regions of the catalyst.

The energy of the interaction between the olefin and Quinoline A in the transition states that lead to the *R* products depends on the olefin chain length. Nevertheless, this behavior is similar to that of the *S* transition state. Therefore, Quinoline A, despite having the highest interaction energies with the olefin, and thus being very important for catalysis, is not critical in determining the enantioselectivity of the reaction.

A qualitative chemical interpretation of the origin of enantioselectivity: Once the relevant regions of the catalyst have been identified, the dependence of the selectivity on the olefin chain length can be explained by the examination of the transition-state structures of the selected conformations. Figure 8 shows the structures of the most stable transition states that lead to the *R* products of propene, 1-hexene, and 1-decene. In all of them, the orientation of the olefin corresponds to that of **B-III**, with the olefin in the binding cleft of the catalyst. By looking at these structures one can see how the elongation of the olefin chain from propene to 1-hexene causes an increase in the interactions between the olefin and the three most important parts of the catalyst, Quinoline A, PYDZ, and Quinuclidine B. From propene to 1-hexene, the carbon atoms added to the aliphatic chain are in close proximity to these three parts of the catalyst, and can interact strongly. In contrast, once the aliphatic *n*-alkene has six carbon atoms, all the carbon atoms subsequently added to the chain are far from the catalyst, and cannot be expected to make strong direct interactions with the catalyst.

The selected conformations that lead to the *S* enantiomer, depicted in Figure 9, show a somewhat different picture. The olefin in all these structures is in the **B-IV** orientation. The aliphatic chain in all of these cases is oriented away from the catalyst's binding cleft. In this orientation, the only part of the catalyst that may directly interact with the aliphatic chain is Quinoline A. In fact, these interactions are reflected in the energy break down shown in Figure 7. The other parts of the catalyst are far away from the aliphatic chain and have minor stabilizing interactions, as shown in the energetic analysis presented in Figure 7.

Looking at the *S* transition states in Figure 9 one can think of other conformations that lead to the *S* enantiomer in which the aliphatic chain is positioned deeper into the binding cleft, thus enhancing the interactions with the catalyst. In fact, we computed these structures during our conformational analysis, and their contribution is included in

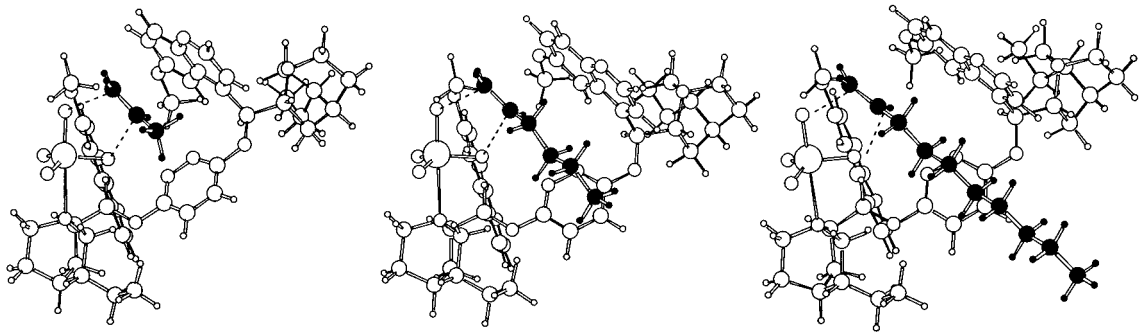

Figure 8. A view of the selected transition states that give the *R* product for propene, 1-hexene, and 1-decene. The olefin is highlighted in black.

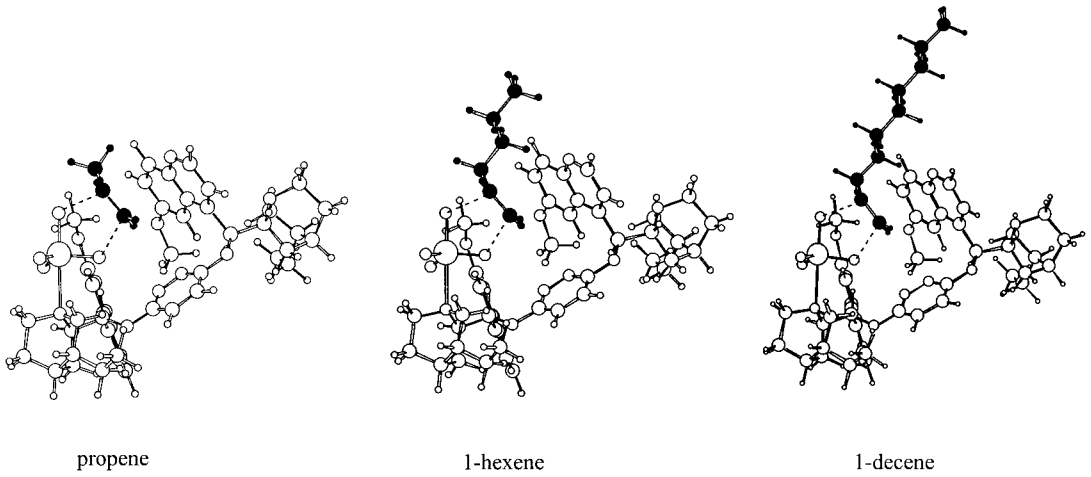

Figure 9. A view of the selected transition states that give the *S* product for propene, 1-hexene, and 1-decene. The olefin is highlighted in black.

the computed enantiomeric excess values. For instance, let us analyze the three most stable *S* conformations of 1-nonene. These three conformations are depicted in Figure 10. The difference in energy between them is less than 0.1 kcal mol^{-1}. Conformation (a) is the selected conformation used in the discussion above; it has the **B-IV** orientation in which the olefin points away from the catalyst. Conformation (b), however, adopts a different olefinic arrangement, with the aliphatic chain placed in the binding cleft of the catalyst. The region of entry of the olefin is the same as that in conformation (a), but here it has the **B-II** orientation. In this case, the interaction energy between the olefin and the catalyst is larger than in conformation (a), but in order to adopt this conformation the olefin has to pay an energy penalty, mainly in terms of torsional and bending energy. This is the reason why, despite the better interactions between the olefin and the catalyst in conformation (b), both conformations (a) and (b) have similar energies. Conformation (c) has a similar total energy to that of the two other conformations. In this case, the interaction energy between the olefin and the catalyst is higher than in conformation (a) since the aliphatic chain is also in the binding cleft of the catalyst. Nevertheless, once again, the olefin is under more tension, like conformation (b), and has a total energy similar to the other conformations. The region of entry of the olefin here is different to that for the other two cases. Conformations (a) and (b) are associated with region **B** whereas conformation (c) has a **C-II** orientation. This example proves that the conformational search was exhaustive, that all the different regions of entry of the olefins were explored, and that all of the conformations were given the chance to contribute to the overall selectivity.

The analysis of these conformations of 1-nonene gives an idea of the difficulties inherent in a detailed analysis of the different conformations that contribute to the enantioselectivity. In this case, for instance, the relative positions of the olefin with respect to the catalyst are completely different for the three conformations although they have similar energies. This is why we decided to analyze in detail only one selected conformation for each of the olefins as this was the only way to obtain information about the catalytic mechanism and the origin of the enantioselectivity.

At this point, we will try to go beyond these numerical and geometrical descriptions and interpret these interactions from a chemical point of view. Examination of the geometries (Figure 8) shows that the relative orientation of the

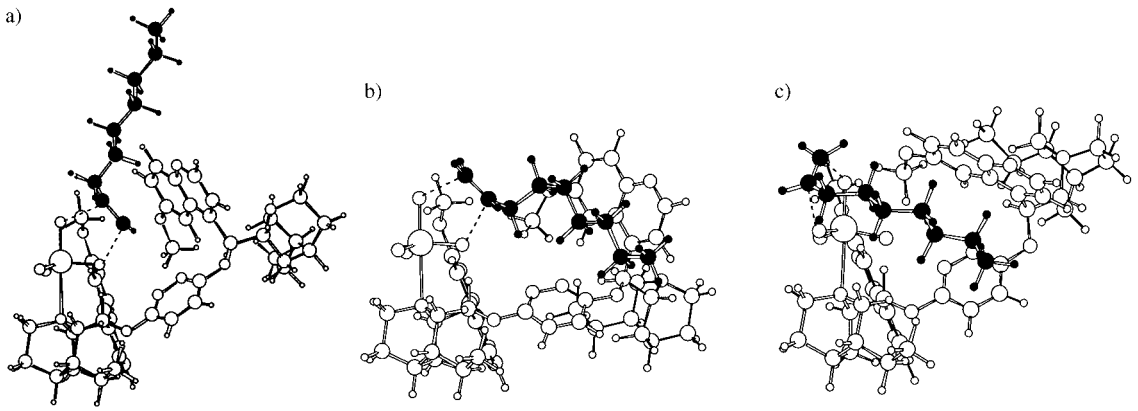

Figure 10. A view of the three most stable transition states giving the *S* product for 1-nonene. The olefin is highlighted in black.

C–H bonds of the olefins and the aromatic walls of the catalyst, especially Quinoline A and PYDZ, can be described as edge-to-face interactions between the C–H bonds of the aliphatic chain and the aromatic walls of the catalyst. Therefore, the main interactions (the most energetic ones) between the aliphatic chain of the alkene and the aromatic rings of the catalyst (PYDZ and Quinoline A) can be described as C–H···π interactions. The other important contribution to the enantioselectivity arises from the interactions between the aliphatic chain of the olefin and Quinuclidine B. These hydrocarbon–hydrocarbon interactions may be attributed to dispersive forces, commonly labeled as hydrophobic interactions.[42]

Attractive interactions between C–H bonds and π systems are well known from structural, conformational and theoretical data.[43–46] These weak interactions are key factors in determining fundamental chemical and biochemical properties, such as the conformational preferences of organic molecules, the stabilization of protein structures and molecular recognition processes.[44] They have also been suggested to play a role in catalyzed dihydroxylation processes.[8b,18b] Attractive interactions of this type are generally attributed to a combination of dispersion forces, and electrostatic and polarization interactions.[47,48] Dispersion forces are generally the most important in this kind of interaction, although electrostatic and polarization interactions sometimes can become more relevant.[49] Hence, albeit the van der Waals term in the MM3 force field does not directly correspond to dispersion forces, this is the term that best represents this kind of interaction.

The C–H···π interactions have previously been described in other reactions as affecting the stereoselectivity. This is the case, for instance, in the hydrogenation of aromatic ketones with a chiral Ru complex. Noyori and co-workers[50] noted that C–H···π interactions between a C–H of a metal ligand and the aromatic ring of the ketone significantly affects the enantioselectivity of the reaction. Other examples in which these interactions are also responsible for determining the stereochemistry include several cycloaddition reactions. For example, the *endo* preference in the Diels–Alder reaction between butadiene and cyclopentene was demonstrated to originate from C–H···π interactions between a C–H of the cyclopentene and the forming double bonds of the butadiene.[51] Similar conclusions were drawn from the study of cyclopropene dimerization.[52]

Conclusions

The IMOMM(Becke3LYP:MM3) computational study of the dihydroxylation of long-chain aliphatic alkenes is much more complicated than that of aromatic alkenes because of the large number of conformations that have to be considered. A procedure has been defined here for the identification and screening of the lowest energy paths. The application of this scheme and the performance of approximately 1700 IMOMM calculations on the conformations of a series of eight aliphatic terminal *n*-alkenes with OsO_4•$(DHQD)_2$-PYDZ yields enantiomeric excesses that closely mimic the experimental values reported for the OsO_4•$(DHQD)_2$-PHAL-catalyzed dihydroxylation of propene, 1-butene, 1-pentene, 1-hexene, and 1-decene. The two most remarkable experimental features, namely the selectivity leading to the *R* product and the dependence of the enantiomeric excess on the length of the aliphatic chain, are satisfactorily reproduced. The analysis of the results, in particular, the partition of the total IMOMM energy into its components, allows the key factors responsible for the selectivity to be identified. The enantioselectivity was found to originate from the C–H···π interactions between the aliphatic chain of the substrate and the aromatic rings of PYDZ, with an important role also being played by Quinuclidine B. Quinoline A, in turn, is critical for catalysis because of its stabilizing C–H···π interactions with the aliphatic chain of the alkenes, but it is not involved in determining the enantioselectivity of the reaction. This behavior is different to that found for aromatic olefins, for which the π···π interactions were shown to be critical, and the critical region of the catalyst was exclusively Quinoline A.

The peculiar relationship between the selectivity and the length of the olefin aliphatic chain can be explained on inspection of the geometries of the most stable transition states. For short chains, an increase in length produces favorable interactions that are exclusive to the *R* enantiomer. In contrast, for longer chains, the chain is lengthened far away from the catalyst and the selectivity is not affected.

Acknowledgements

Financial support from the Spanish DGES through Project No. BQU-2002–04110-C02–02 is acknowledged. The use of the computational facilities at the Centre de Supercomputació de Catalunya (C4) is appreciated. G.U. acknowledges the Spanish MCYT for funding through the "Ramón y Cajal" Program. F.M. thanks the Catalan DURSI for financial support, as well as the ICIQ foundation. G.D.-S. acknowledges the Spanish MECD for financial support.

[1] K. B. Sharpless, *Angew. Chem.* **2002**, *114*, 2126; *Angew. Chem. Int. Ed.* **2002**, *41*, 2024.
[2] a) *Applied Homogeneous Catalysis with Organometallic Compounds* (Eds.: B. Cornils, W. A. Herrmann), Wiley-VCH, Weinheim, **2002**; b) *Catalytic Asymmetric Synthesis* (Ed.: I. Ojima), Wiley-VCH, Weinheim, **1993**.
[3] *Transition Metals in Organic Synthesis* (Eds.: M. Beller, C. Bolm), Wiley-VCH, Weinheim, **1998**.
[4] B. B. Lohray, *Tetrahedron: Asymmetry* **1992**, *3*, 1317.
[5] H. C. Kolb, M. S. VanNieuwenhze, K. B. Sharpless, *Chem. Rev.* **1994**, *94*, 2483.
[6] a) C. Döbler, G. M. Mehltretter, U. Sundermeier, M. Beller, *J. Am. Chem. Soc.* **2000**, *122*, 10289; b) S. Y. Jonsson, K. Färnegårdh, J.-E Bäckwall, *J. Am. Chem. Soc.* **2001**, *123*, 1365; c) B. M. Choudary, N. S. Chowdari, K. Jyothi, M. L. Kantam, *J. Am. Chem. Soc.* **2002**, *124*, 5341; d) A. Severeyns, D. E. De Vos, L. Fiermans, F. Verpoort, P. J. Grobet, P. A. Jacobs, *Angew. Chem.* **2001**, *113*, 606; *Angew. Chem. Int. Ed.* **2001**, *40*, 586; e) M. A. Andersson, R. Epple, V. V. Fokin, K. B. Sharpless, *Angew. Chem.* **2002**, *114*, 490; *Angew. Chem. Int. Ed.* **2002**, *41*, 472.

[7] a) E. J. Corey, M. C. Noe, S. Sarshar, *J. Am. Chem. Soc.* **1993**, *115*, 3828; b) E. J. Corey, A. Guzman-Perez, M. C. Noe, *J. Am. Chem. Soc.* **1994**, *116*, 12109; c) E. J. Corey, M. C. Noe, *J. Am. Chem. Soc.* **1996**, *118*, 319.

[8] a) T. Göbel, K. B. Sharpless, *Angew. Chem.* **1993**, *105*, 1329; *Angew. Chem. Int. Ed. Engl.* **1993**, *32*, 1329; b) H. C. Kolb, P. G. Andersson, K. B. Sharpless, *J. Am. Chem. Soc.* **1994**, *116*, 1278; c) P.-O. Norrby, H. Becker, K. B. Sharpless, *J. Am. Chem. Soc.* **1996**, *118*, 35.

[9] a) M. Nakajima, K. Tomioka, Y. Iitaka, K. Koga, *Tetrahedron* **1993**, *49*, 10793; b) P.-O. Norrby, K. P. Gable, *J. Chem. Soc., Perkin Trans. 2*, **1996**, 171.

[10] a) S. Dapprich, G. Ujaque, F. Maseras, A. Lledós, D. G. Musaev, K. Morokuma, *J. Am. Chem. Soc.* **1996**, *118*, 11660; b) U. Pidun, C. Boehme, G. Frenking, *Angew. Chem.* **1996**, *108*, 3008; *Angew. Chem. Int. Ed. Engl.* **1996**, *35*, 2817; c) M. Torrent, L. Deng, M. Duran, M. Solà, T. Ziegler, *Organometallics* **1997**, *16*, 13; d) A. J. Del Monte, J. Haller, K. N. Houk, K. B. Sharpless, D. A. Singleton, T. Strassner, A. A. Thomas, *J. Am. Chem. Soc.* **1997**, *119*, 9907; e) T. Strassner in *Computational Modeling of Homogeneous Catalysis* (Eds.: F. Maseras, A. Lledós), Kluwer, Dordrecht, **2002**.

[11] D. V. Deubel, G. Frenking, *Acc. Chem. Res.* **2003**, *36*, 645.

[12] G. Ujaque, F. Maseras, A. Lledós, *Eur. J. Org. Chem.* **2003**, *5*, 833.

[13] D. V. Deubel, S. Schlecht, G. Frenking, *J. Am. Chem. Soc.* **2001**, *123*, 10085; b) D. V. Deubel, *J. Phys. Chem. A* **2002**, *106*, 431.

[14] a) D. P. Gable, J. J. J. Juliette, *J. Am. Chem. Soc.* **1996**, *118*, 2625; b) K. P. Gable, A. AbuBaker, K. Zientara, A. M. Wainwright, *Organometallics* **1999**, *18*, 173; c) K. P. Gable, F. A. Zhuravlev, *J. Am. Chem. Soc.* **2002**, *124*, 3970.

[15] G. Ujaque, F. Maseras, A. Lledós, *J. Am. Chem. Soc.* **1999**, *121*, 1317.

[16] a) G. Ujaque, F. Maseras, A. Lledós, *J. Org. Chem.* **1997**, *62*, 7892; b) G. Ujaque, F. Maseras, A. Lledós, *Theor. Chim. Acta* **1996**, *94*, 67.

[17] J. Haller, T. Strassner, K. N. Houk, *J. Am. Chem. Soc.* **1997**, *119*, 8031.

[18] a) P.-O. Norrby, T. Rasmussen, J. Haller, T. Strassner, K. N. Houk, *J. Am. Chem. Soc.* **1999**, *121*, 10186; b) P. Fristrup, D. Tanner, P.-O. Norrby, *Chirality* **2003**, *15*, 360.

[19] a) N. Moitessier, B. Maigret, F. Chretien, Y. Chapleur, *Eur. J. Org. Chem.* **2000**, 995; b) N. Moitessier, C. Henry, C. Len, Y. Chapleur, *J. Org. Chem.* **2002**, *67*, 7275.

[20] H. Becker, S. B. King, M. Taniguchi, K. P. M. Vanhessche, K. B. Sharpless, *J. Org. Chem.* **1995**, *60*, 3940.

[21] a) G. A. Crispino, A. Makita, Z.-M. Wang, K. B. Sharpless, *Tetrahedron Lett.* **1994**, *35*, 543; b) E. J. Corey, M. C. Noe, *J. Am. Chem. Soc.* **1996**, *118*, 11038.

[22] F. Maseras, K. Morokuma, *J. Comput. Chem.* **1995**, *16*, 1170.

[23] a) M. Svensson, S. Humbel, R. D. J. Froese, T. Matsubara, S. Sieber, K. Morokuma, *J. Phys. Chem.* **1996**, *100*, 19357; b) S. Dapprich, I. Komaromi, K. S. Byun, K. Morokuma, M. J. Frisch, *J. Mol. Struct.* **1999**, *461–462*, 1; c) T. Vreven, K. Morokuma, Ö. Farkas, H. B. Schlegel, M. J. Frisch, *J. Comput. Chem.* **2003**, *24*, 760.

[24] *Computational Modeling of Homogeneous Catalysis* (Eds.: F. Maseras, A. Lledós), Kluwer, Dordrecht, **2002**.

[25] F. Maseras, *Chem. Commun.* **2000**, 1821.

[26] a) D. Gleich, W. A. Herrmann, *Organometallics* **1999**, *18*, 4354; b) B. Goldfuss, M. Steigelmann, S. I. Khan, K. N. Houk, *J. Org. Chem.* **2000**, *65*, 77; c) S. Feldgus, C. R. Landis, *J. Am. Chem. Soc.* **2000**, *122*, 12714; d) E. Jacobsen, L. Cavallo, *Chem. Eur. J.* **2001**, *7*, 800; e) D. V. Khoroshun, D. G. Musaev, T. Vreven, K. Morokuma, *Organometallics* **2001**, *20*, 2007; f) J. J. Carbó, F. Maseras, C. Bo, P. W. N. M. van Leeuwen, *J. Am. Chem. Soc.* **2001**, *123*, 7630; g) S. Tobisch, T. Ziegler, *J. Am. Chem. Soc.* **2002**, *124*, 13290; h) C. Adlhart, P. Chen, *Angew. Chem.* **2002**, *114*, 4668; *Angew. Chem. Int. Ed.* **2002**, *41*, 4484.

[27] Gaussian 98, Revision A.9, M. J. Frisch, G. W. Trucks, H. B. Schlegel, G. E. Scuseria, M. A. Robb, J. R. Cheeseman, V. G. Zakrzewski, J. A. Montgomery, Jr., R. E. Stratmann, J. C. Burant, S. Dapprich, J. M. Millam, A. D. Daniels, K. N. Kudin, M. C. Strain, O. Farkas, J. Tomasi, V. Barone, M. Cossi, R. Cammi, B. Mennucci, C. Pomelli, C. Adamo, S. Clifford, J. Ochterski, G. A. Petersson, P. Y. Ayala, Q. Cui, K. Morokuma, D. K. Malick, A. D. Rabuck, K. Raghavachari, J. B. Foresman, J. Cioslowski, J. V. Ortiz, B. B. Stefanov, G. Liu, A. Liashenko, P. Piskorz, I. Komaromi, R. Gomperts, R. L. Martin, D. J. Fox, T. Keith, M. A. Al-Laham, C. Y. Peng, A. Nanayakkara, C. Gonzalez, M. Challacombe, P. M. W. Gill, B. Johnson, W. Chen, M. W. Wong, J. L. Andres, C. Gonzalez, M. Head-Gordon, E. S. Replogle, J. A. Pople, Gaussian, Inc., Pittsburgh, PA, **1998**.

[28] N. L. Allinger, MM3(92), QCPE, Bloomington, IN, **1992**.

[29] a) A. D. Becke, *J. Chem. Phys.* **1993**, *98*, 5648; b) D. Lee, W. Yang, R. G. Parr, *Phys. Rev. B* **1988**, *37*, 785; c) P. J. Stephens, F. J. Devlin, C. F. Chabalowski, M. J. Frisch, *J. Phys. Chem.* **1994**, *98*, 11623.

[30] a) N. L. Allinger, Y. H. Yuh, J. H. Lii, *J. Am. Chem. Soc.* **1989**, *111*, 8551; b) J. H. Lii, N. L. Allinger, *J. Am. Chem. Soc.* **1989**, *111*, 8566; c) J. H. Lii, N. L. Allinger, *J. Am. Chem. Soc.* **1989**, *111*, 8576.

[31] A. K. Rappé, C. J. Casewit, D. S. Colwell, W. A. Goddard III, W. N. Skiff, *J. Am. Chem. Soc.* **1992**, *114*, 10024.

[32] P. C. Hariharan, J. A. Pople, *Theor. Chim. Acta* **1973**, *28*, 213.

[33] W. J. Hehre, R. Ditchfield, J. A. Pople, *J. Chem. Phys.* **1972**, *56*, 2257.

[34] P. J. Hay, W. R. Wadt, *J. Chem. Phys.* **1985**, *82*, 299.

[35] G. Ujaque, F. Maseras, A Lledós, *Int. J. Quantum Chem.* **2000**, *77*, 544.

[36] A. W. Ehlers, M. Böme, S. Dapprich, A. Gobbi, A. Höllwarth, V. Jonas, K. F. Köler, R. Stegmann, A. Veldkamp, G. Frenking, *Chem. Phys. Lett.* **1993**, *208*, 111.

[37] E. J. Corey, M. C. Noe, *J. Am. Chem. Soc.* **1993**, *115*, 12579.

[38] a) G. D. H. Dijkstra, R. M. Kellogg, H. Wynberg, J. S. Svendsen, I. Marko, K. B. Sharpless, *J. Am. Chem. Soc.* **1989**, *111*, 8069; b) P.-O. Norrby, H. C. Kolb, K. B. Sharpless, *J. Am. Chem. Soc.* **1994**, *116*, 8470.

[39] A. G. Leach, *Molecular Modelling, Principles and Applications*, 2nd ed., Pearson Education Limited, Harlow, **2001**, p. 458.

[40] D. Gleich, R. Schmid, W. A. Herrmann, *Organometallics* **1998**, *17*, 4828.

[41] G. Ujaque, F. Maseras, O. Eisenstein, *Theor. Chem. Acc.* **1997**, *96*, 146.

[42] L. R. Pratt, A. Pohorille, *Chem. Rev.* **2002**, *102*, 2671 , and references therein.

[43] M. Nishio, Y. Umezawa, M. Hirota, Y. Takeuchi, *Tetrahedron* **1995**, *51*, 8665.

[44] a) M. Nishio, M. Hirota, Y. Umezawa, *The C-H/π interaction: Evidence, Nature and Consequences*, Wiley-VCH, New York, **1999**; b) G. R. Desiraju, T. Steiner, *The Weak Hydrogen Bond in Structural Chemistry and Biology*, Oxford University Press, Oxford, **1999**.

[45] M. J. Calhorda, *Chem. Commun.* **2000**, 801.

[46] S. Sakaki, K. Kato, T. Miyazaki, Y. Musashi, K. Ohkubo, H. Ihara, C. Hirayama, *J. Chem. Soc., Faraday Trans.* **1993**, *89*, 659.

[47] S. Tsuzuki, K. Honda, U. Tadafumi, M. Mikami, K. Tanabe, *J. Am. Chem. Soc.* **2000**, *122*, 3746.

[48] J. Ribas, E. Cubero, F. J. Luque, M. Orozco, *J. Org. Chem.* **2002**, *67*, 7057.

[49] G. Ujaque, P. S. Lee, K. N. Houk, M. F. Hentemann, S. J. Danishefsky, *Chem. Eur. J.* **2002**, *8*, 3423.

[50] M. Yamakawa, I. Yamada, R. Noyori, *Angew. Chem.* **2001**, *113*, 2900; *Angew. Chem. Int. Ed.* **2001**, *40*, 2818.

[51] M. Sodupe, R. Rios, V. Branchadell, T. Nicholas, A. Oliva, J. J. Dannenberg, *J. Am. Chem. Soc.* **1997**, *119*, 6902.

[52] Q. Deng, B. E. Thomas, K. N. Houk, P. Dowd, *J. Am. Chem. Soc.* **1997**, *119*, 6902.

Received: March 1, 2004
Revised: September 10, 2004
Published online: December 21, 2004

